Cerebral Circulation - Cognition and Behavior 6 (2024) 100218

Contents lists available at ScienceDirect

Cerebral Circulation - Cognition and Behavior

journal homepage: www.sciencedirect.com/journal/cerebral-circulation-cognition-and-behavior

Cortical microstructural involvement in cerebral small vessel disease

Annemarie Reiländer [a,b,1], Marlene Engel [a,1], Ulrike Nöth [b], Ralf Deichmann [b], Manoj Shrestha [b], Marlies Wagner [b,c], René-Maxime Gracien [a,b], Alexander Seiler [b,d,e,*]

[a] Department of Neurology, Goethe University Hospital, Frankfurt, Germany
[b] Brain Imaging Center, Goethe University, Frankfurt, Germany
[c] Institute of Neuroradiology, Goethe University Hospital, Frankfurt, Germany
[d] Department of Neurology, University Hospital Schleswig-Holstein, Kiel, Germany
[e] Neurovascular Center, University Hospital Schleswig-Holstein, Kiel, Germany

ARTICLE INFO

Keywords:
Small vessel disease
Cortical microstructure
Diffusion tensor imaging
quantitative MRI
Brain atrophy
Microstructural impairment

ABSTRACT

Background: In cerebral small vessel disease (CSVD), cortical atrophy occurs at a later stage compared to microstructural abnormalities and therefore cannot be used for monitoring short-term disease progression. We aimed to investigate whether cortical diffusion tensor imaging (DTI) and quantitative (q) magnetic resonance imaging (MRI) are able to detect early microstructural involvement of the cerebral cortex in CSVD.

Materials and Methods: 33 CSVD patients without significant cortical or whole-brain atrophy and 16 healthy control subjects were included and underwent structural MRI, DTI and high-resolution qMRI with T_2, T_2* and $T_{2'}$ mapping at 3 T as well as comprehensive cognitive assessment. After tissue segmentation and reconstruction of the cortical boundaries with the Freesurfer software, DTI and qMRI parameters were saved as surface datasets and averaged across all vertices.

Results: Cortical diffusivity and quantitative T_2 values were significantly increased in patients compared to controls ($p < 0.05$). T_2 values correlated significantly positively with white matter hyperintensity (WMH) volume ($p < 0.01$). Both cortical diffusivity and T_2 showed significant negative associations with axonal damage to the white matter fiber tracts ($p < 0.05$).

Conclusions: Cortical diffusivity and quantitative T_2 mapping are suitable to detect microstructural involvement of the cerebral cortex in CSVD and represent promising imaging biomarkers for monitoring disease progression and effects of therapeutical interventions in clinical studies.

Introduction

Cerebral small vessel disease (CSVD) has been identified as the underlying etiology in approximately 20 % of all ischemic strokes and is the major cause of vascular dementia [1]. Furthermore, SVD has been proposed as an important propagator of cerebral Alzheimer's pathology in individuals with vascular risk factors [2,3]. Apart from lacunes and cerebral microbleeds (CMB), it manifests itself with white matter hyperintensities (WMH) as the predominant finding on conventional magnetic resonance imaging (MRI) [1,4,5].

Further to an impairment of the subcortical (micro-)structural tissue integrity, the occurrence of brain atrophy - including atrophy of the cortical grey matter [6] - is a widely acknowledged feature of CSVD [7–9]. It has been generally proposed as a surrogate marker of disease progression [7,8]. Volume reduction of the entire brain and its progression over time account for some of the cross-sectional and longitudinal variance in cognitive function in CSVD patients [7]. Progressive and accelerated brain atrophy compared to healthy control subjects has

Abbreviations: CSVD, Cerebral small vessel disease; CMB, Cerebral microbleeds; WMH, White matter hyperintensities; qMRI, Quantitative magnetic resonance imaging; DTI, Diffusion tensor imaging; FLAIR, Fluid-attenuated inversion recovery; WM, White matter; T, Tesla; RF, Radio-frequency; DW, Diffusion-weighted; tr, Twice-refocused; SE, Spin echo; EPI, Echoplanar imaging; BW, Bandwidth; TR, Repetition time; TE, echo time; FOV, field-of-view; MP-RAGE, Magnetization-Prepared Rapid Acquisition of Gradient Echos; FA, fractional anisotropy; MD, mean diffusivity; RD, radial diffusivity; CERAD, Consortium to Establish a Registry for Alzheimer's Disease; MMSE, Mini-Mental State Examination; TMT, trail making test; NBV, normalized brain volume.

* Corresponding author at: Department of Neurology, University Hospital Schleswig-Holstein, Campus Kiel, Arnold-Heller-Straße 7, 24105 Kiel, Germany.
E-mail address: Alexander.Seiler@uksh.de (A. Seiler).

[1] These authors contributed equally to this work.

https://doi.org/10.1016/j.cccb.2024.100218

Available online 11 March 2024

been demonstrated in longitudinal imaging studies on patients with CSVD [6,7,10]. However, a decrease of the cerebral volume fraction seems to follow progression of WMH and microstructural damage to the cerebral white matter as detected by diffusion tensor imaging (DTI) parameters and therefore presumably represents a secondary phenomenon [10]. Consequently, since tissue atrophy occurs at a later stage, thus yielding lower effect sizes compared to WMH progression and the impairment of the white matter microstructure [10], it might be a less sensitive imaging marker for monitoring short-term disease progression or the effects of therapeutical interventions in patients with CSVD [10]. Furthermore, normal aging has been shown to yield similar effects: it is likewise associated with progressive cortical atrophy, showing spatial patterns that are similar to the regional distribution of cortical thinning found in CSVD [11], and mediates a negative relationship between WMH volume and cortical thickness [11,12]. In fact, some studies reported no significant association between the global or regional WMH volume and cortical thickness when controlling for age [9,13,14]. For these reasons, other imaging parameters might be more promising for both detecting and monitoring cortical microstructural damage in CSVD.

The findings of previous studies suggest that DTI parameters may be useful for detecting the impairment of neuronal fibers and microstructural boundaries in cortical tissue [15,16]. According to the results of previous studies, quantitative mapping of the reversible (T_2), irreversible (T_2') and the effective (T_2*) transverse relaxation times might also provide promising imaging biomarkers for specifically detecting the actual cortical tissue pathology in CSVD [17,18]. Therefore, we hypothesized that common DTI parameters and the qMRI-based parameters T_2, T_2* and $T_{2'}$ might allow for the characterization of microstructural cortical tissue damage in CSVD. We further hypothesized that these imaging parameters might be more sensitive for detecting an early impairment of the cortical microstructural integrity than measurements of tissue atrophy, thus adding useful information with regard to the microstructural processes underlying cortical microstructural involvement in CSVD. In this study, cortical qMRI and DTI parameters were investigated in a surface-based manner along with parameters reflecting brain and cortical atrophy in CSVD patients and age-matched healthy control subjects. Furthermore, we tested whether the listed imaging parameters for assessing the cortical microstructural integrity are associated with the extent of white matter damage and cognitive performance in CSVD.

Material and methods

Subjects

Patients with sporadic CSVD (n = 33) were recruited from our neurological department and the integrated academic stroke center. CSVD was defined as the presence of confluent WMH (Fazekas $\geq$ 2) and lacunes on T2-weighted/FLAIR MRI [3]. The patients had been admitted to hospital with either acute neurological symptoms (ischemic stroke or transient ischemic attack with a typical lacunar syndrome (n = 16)) or chronic neurological symptoms attributable to CSVD (such as cognitive decline or gait impairment (n = 3)), or had shown confluent WMH as an incidental finding on neuroimaging (n = 14). The latter subjects came to attention in the course of imaging-based diagnostics of transient neurological symptoms such as e.g. dizziness or headache. Those subjects were only be enrolled if thorough evaluation based on all available diagnostic information did not reveal any evidence of an acute or chronic neurological disease.

Exclusion criteria were: cognitive impairment or dementia with suspicion of a neurodegenerative origin (according to clinical criteria such as additional movement or behavioral disorder, prominent 'cortical' dementia with predominant memory deficits or speech abnormalities as well as according to neuroimaging findings indicating regional atrophy patterns compatible with a neurodegenerative condition such as Alzheimer's disease), stenosis of a brain-supplying artery with a degree exceeding $\geq$ 50 %, non-lacunar stroke and white matter lesions suggestive for an alternative etiology (e.g. inflammatory). A group of healthy control subjects (n = 16) was recruited by public and word-of-mouth advertising. Matching for age and sex between the groups was performed according to the proportion of subjects of a certain age and sex present in the CSVD patient group. Control subjects were recruited accordingly with the objective to achieve the same percentage distribution for age and sex as in the patient group.

Eligibility as control subject required a medical history free from neurological and psychiatric diseases and common vascular risk factors (apart from controlled arterial hypertension), and the absence of confluent white matter hyperintensities on FLAIR imaging (Fazekas $\leq$ 1) [3,17]. The study was approved by the local institutional review board of the Goethe University Frankfurt (Faculty of Medicine) and conducted in accordance with the Declaration of Helsinki (revised version from 1983). Written informed consent was obtained from all subjects before inclusion in the study. The patients and control subjects in this study overlap with the subjects described in a previously published work [17].

MR imaging protocol

MRI data acquisition was performed on a 3-Tesla (T) whole-body magnetic resonance (MR) scanner (Trio, Siemens Healthineers, Erlangen, Germany) which uses a body coil for radio-frequency (RF) transmission and an 8-channel phased-array head coil for RF reception. Imaging data were acquired on a single scanner using the identical imaging protocol for all participants.

DTI data were acquired using a diffusion-weighted (DW) twice-refocused (tr) spin-echo (SE) echo planar imaging (EPI) sequence. Parameters used for DTI data acquisition were: field of view (FoV) = 192 × 192 mm^2, matrix size = 96 × 96, isotropic resolution = 2 mm, 70 interleaved axial slices (2 mm thickness, no interslice gap), TR = 9000 ms, TE = 81 ms, echo-spacing =0.8 ms, readout bandwidth (BW) = 1371 Hz/pixel, partial Fourier encoding = 6/8, parallel imaging with two-fold acceleration, 12 different diffusion encoding directions with a b-value of 1000s/mm^2. To correct for geometrical distortions induced by static magnetic field (B0) inhomogeneities, two sets of five reference images with b = 0 were acquired with either positive or negative phase encoding gradients, yielding five pairs of DTI data sets with opposite distortions. The total duration was 4:13 min.

T_2 mapping was based on a fast spin-echo sequence with an echo-train length of 11 echoes per excitation, an echo spacing of 17.1 ms, and the following imaging parameters: 25 axial slices (2 mm thickness, 1 mm interslice gap), TR = 5000 ms, BW = 100 Hz/pixel, 180° refocusing pulses, FOV = 240 × 180 mm^2, matrix size = 192 × 144 (readout × phase encoding), in-plane resolution = 1.25 × 1.25 mm^2. For quantitative T_2 mapping, 5 datasets were acquired with different TE values (17, 86, 103, 120, 188 ms), keeping all other acquisition parameters constant. The total duration was 6:25 min.

Mapping of T_2* was based on the acquisition of eight multiple-echo gradient echo (GE) datasets with export of phase and modulus data: FOV = 240×180 mm^2, matrix size = 192 × 144 (readout × phase encoding), in-plane resolution = 1.25 × 1.25 mm^2, 25 axial slices, slice thickness = 2 mm, inter-slice gap = 1 mm, TE = [10,16,22,28,34,40,46,52] ms, TR = 1500 ms, excitation angle (α) = 30°, BW = 299 Hz/Pixel, duration = 3:36 min.

For motion correction, the acquisition was repeated twice with reduced spatial resolution (and therefore reduced k-space coverage) in phase encoding direction, covering only the central 50 % (duration = 1:57 min) and 25 % (duration = 1:03 min) of k-space.

Anatomical imaging for tissue segmentation and reconstruction of the cortical surface and cortical boundaries was based on a T1-weighted Magnetization-Prepared Rapid Acquisition of Gradient Echos (MP-RAGE) data set, acquired with the following parameters: TR/TE/TI = 1900/3.04/900 ms, FOV = 256 × 256 × 192 mm^3, matrix size =

256 × 256 × 192, whole-brain coverage, isotropic spatial resolution =1 mm, α = 9°, BW = 170 Hz/pixel, duration = 4:28 min. Furthermore, a 3D FLAIR sequence was included for the segmentation of WMH. Protocol parameters were: TR/TE/TI = 6000/353/2200 ms, FOV = 250 × 215 × 160 mm^3, matrix = 256 × 220 × 80, interpolated to 256 × 220 × 160, whole-brain coverage, isotropic spatial resolution = 1 mm, duration = 8:08 min.

Image post-processing and analysis

Imaging data were processed with custom-built MATLAB programs (version 8.0, The MathWorks, Inc.) and shell scripts employing tools from the FMRIB's Software Library (FSL, version 5.0.7) [19] and the Freesurfer toolbox [20].

The DTI data with positive and negative phase encoding gradients were processed with the FSL tool 'TOPUP' [21], estimating the susceptibility-induced B0 inhomogeneities with subsequent distortion correction of the DTI data [21]. Skull-stripping of the corrected data and the creation of a binary brain mask was performed with the FSL tool 'BET' [22]. Using default parameters, corrections inside the brain mask were performed with the FSL tool 'EDDY' [23] to compensate for residual eddy-current-induced distortions and subject motion effects. The water diffusion tensor for each voxel and parametric maps of the fractional anisotropy (FA), mean diffusivity (MD) and radial diffusivity (RD) calculated from the local diffusion tensor eigenvalues were obtained with the FSL tool 'DTIFIT' [24,25]. RD was quantified in addition to the more common DTI parameters FA and MD as it represents the average diffusion perpendicular to the principal axis of the diffusion tensor, which is likely to be particularly sensitive to microstructural damage affecting microstructural boundaries such as membrane and myelin structures (in contrast to axonal structures) [26–28]. For this reason, we hypothesized that RD might be especially suited for the detection of pathological tissue changes of the cerebral cortex in CSVD.

T_2 and T_2* mapping was performed via mono-exponential fitting of the signal in the series of FSE (T2) or GE (T2*) data sets obtained with multiple TE. T_2* mapping included an algorithm for subject motion correction [29], replacing motion-affected lines in k-space by the respective lines acquired in the additional data sets with reduced k-space sampling. The effects of B0 distortions were eliminated from the T2*-weighted data. T_2* maps were co-registered to the T_2 maps (six degrees of freedom). $T_{2'}$ maps were derived from T_2* and T_2 maps according to the formula: $1/T_{2'} = 1/T_2^* - 1/T_2$.

WMH were automatically segmented on skull-stripped FLAIR images (Fig. 1, upper left image). In brief, a custom-built MATLAB script employing functions from the MRIcron software (Chris Rorden, Columbia, SC, USA; www.mricro.com) was used to segment the WMH based on FLAIR signal intensities and histogram analyses as described earlier in detail [17]. If necessary, the WMH segmentations were corrected manually by two experienced neurological/neuroradiological readers, who also evaluated from the structural imaging data the individual Fazekas score (calculated as the mean score of the periventricular and the deep white matter) as well as the number of lacunes and CMBs in each subject. During this procedure, standardized consensus criteria were applied for the identification and assignment of the respective lesions based on the FLAIR, T1- and T2*-weighted images [5]. Based on the evaluated and corrected individual WMH segmentation (Fig. 1, lower left image), the total WMH volume was calculated for each subject.

Structural T1-weighted images were processed with the Freesurfer "recon-all" stream for tissue segmentation [20], including reconstruction of the cortical ribbon and its boundaries and vertex-wise measurement of the cortical thickness. The normalized brain volume (NBV) was calculated as the segmented entire brain volume divided by the total intracranial volume (TIV). Mean cortical thickness was calculated

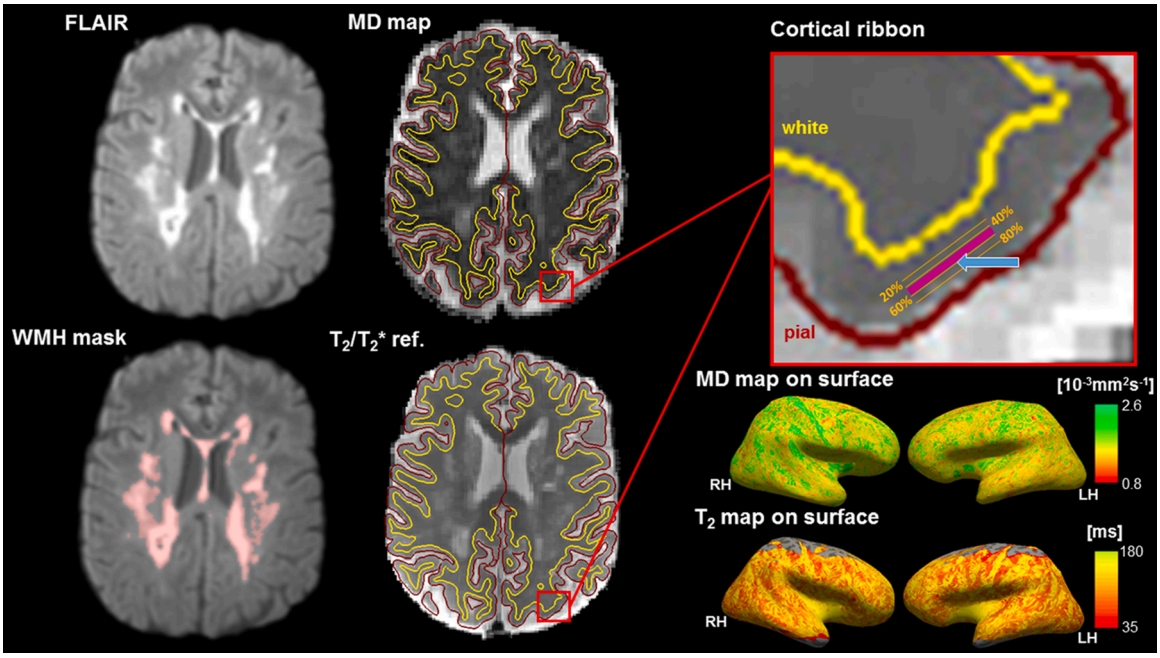

Fig. 1. Left: Representative FLAIR image used for segmentation of WMH (top) and FLAIR image with segmented binary WMH mask, shown as overlay (bottom, red). **Centre:** Data used for registration to the individual anatomical image: MD map (top) and T_2/T_2* reference images (bottom). Data are shown after boundary-based registration to the individual anatomical image with the inner (white matter surface, yellow) and the outer (pial surface, red) cortical boundary shown as surface overlays.

Right: Illustration of the approach used for boundary-based registration of the DTI and qMRI parameter maps and subsequent reading of the parameter values. Using the respective coregistration matrices, DTI and qMRI parameter values were extracted from the middle of the cortical layer (projection fraction of 0.4–0.6, corresponding to the middle 20 % of the cortical ribbon) (top, pink area, blue arrow). MD and T_2 maps are shown on the inflated cortical surface after sampling to the middle 20 % of the cortical ribbon (bottom). Note that data for T_2, T_2* and $T_{2'}$ mapping were not acquired with full brain coverage. mm: millimeters; s: seconds; ms: milliseconds; RH: right hemisphere; LH: left hemisphere.

hemisphere-wise by averaging across all vertices in the cortical thickness surface data sets provided by "recon-all" and the mean global thickness was obtained by calculating the mean of both hemispheres.

For spatial alignment of the EPI-based DTI data and qMRI parameter maps with the T1-weighted structural images we used boundary-based registration with the tool "BBREGISTER", as included in the Freesurfer software. This coregistration method is based on fitting the WM boundaries of the structural image and aligning the results with the EPI, respectively qMRI data. Advantages of this method have been shown in terms of avoiding partial volume effects, thereby minimizing spurious contributions from the adjacent cerebrospinal fluid (CSF) and the cerebral white matter during the analysis of quantitative imaging parameters of different modalities in the thin cortical ribbon [30,31]. In a first step, MD maps and the T_2/T_2* reference images were coregistered to the individual T1-weighted image (Fig. 1), as they have favourable contrast properties. Afterwards, the resulting coregistration matrices were applied to the (remaining) DTI and qMRI parametric maps, respectively. After boundary-based registration to the individual T1-weighted structural image (Fig. 2), DTI and qMRI parameter maps of each subject were stored as surface datasets with a high resolution (~1 mm distance between the vertices). Subsequently, the respective coregistration matrices were applied to read DTI and qMRI parameter values from the middle of the cortical layer (projection fraction of 0.4–0.6, corresponding to the middle 20 % of the cortical ribbon) for further reduction of partial volume effects (Fig. 1, right images). The DTI and qMRI parameter values were extracted from all vertices for calculating averaged global parameter values for the entire cortical surface. The individual WM segmentation obtained with "recon-all" was transformed into a binary mask and used to extract global averaged FA values across the entire cerebral WM as a marker of axonal damage from the coregistered FA maps.

Cognitive assessment

Cognitive assessment was performed by an experienced investigator blinded to the relevant clinical and imaging data of the respective subjects, using the German version of the test battery of the Consortium to Establish a Registry for Alzheimer's Disease (CERAD, CERAD-plus version) [32]. A freely available software (https://www.memoryclinic.ch) was used to transform the raw scores from the CERAD-plus battery into z-scores corrected for age, sex and years of education, based on two normative samples for the German CERAD-plus version [33]. In order to reduce the number of tests for the statistical analyses and to produce more robust results for the cognitive measures, two cognitive composite scores were constructed by averaging the z-scores of multiple subtests [7]. First, as a measure of global cognition, we calculated a global cognitive composite score similar to the CERAD total score described by Chandler et al. [34] by averaging the corrected z-scores of the CERAD subtests, excluding the Mini-Mental State Examination (MMSE). In addition, an executive function composite score was calculated by averaging the z-scores of the verbal fluency test and the 'subcortical' cognitive domains in the CERAD-plus battery, which include the trail making test parts A and B (TMT-A, TMT-B), the ratio TMT-B/A and the 's-words' test.

Statistical analysis

Statistical analyses were performed with IBM SPSS 27 (Armonk, NY). After testing for normal distribution with the Kolmogorov-Smirnov-test, we applied unpaired *t*-tests for group comparisons of imaging parameters and cognitive scores. Evaluation for equality of variance of the data between the groups was performed with the Levene-test. Due to the skewed distribution, WMH volumes were log-transformed for further statistical analyses [12,35]. Associations of imaging parameters with WM lesion load and the extent of microstructural WM damage, as well as with cognitive scores, were assessed by partial correlation analyses controlling for age and sex. Statistical significance was set to $p < 0.05$.

Results

Demographic baseline characteristics, findings from structural imaging and cognitive performance in SVD patients and control subjects

CSVD patients ($n = 33$) and control subjects ($n = 16$) did not differ in terms of age and sex ($p = 0.925$ and $p = 0.610$). Furthermore, there was no statistically significant difference concerning the structural imaging

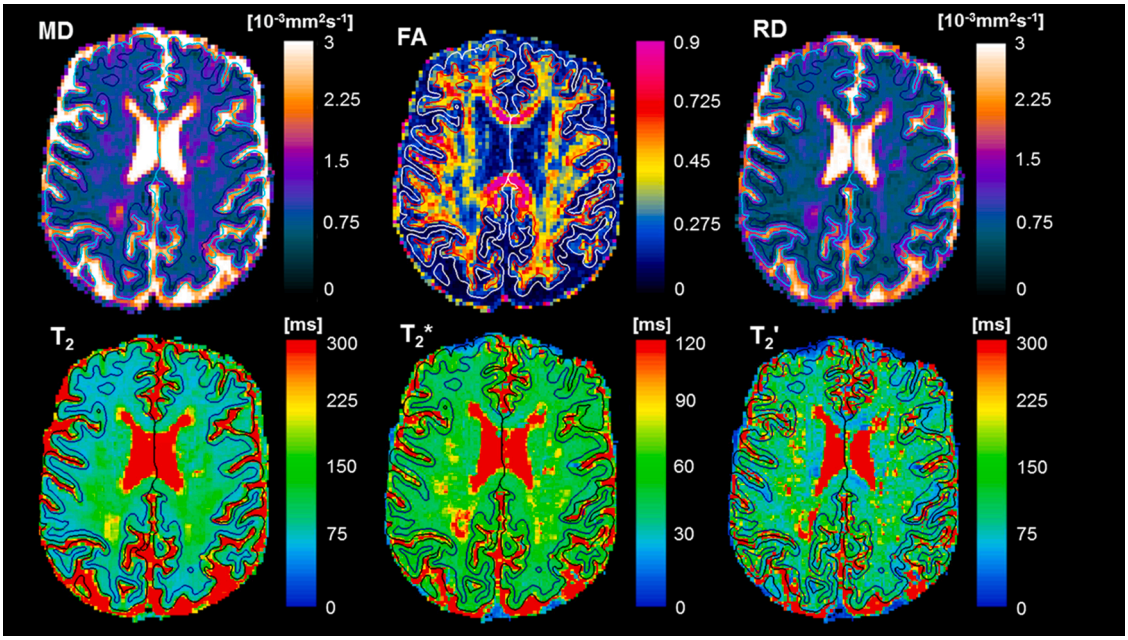

Fig. 2. Imaging parameter maps shown after boundary-based registration to the individual anatomical image with the inner (white matter surface) and the outer (pial surface) cortical boundary shown as surface overlays (same patient as in Fig. 1). Upper row: DTI parameter maps; lower row: qMRI parameter maps. MD: mean diffusivity; FA: fractional anisotropy; RD: radial diffusivity; mm: millimeters; s: seconds; ms: milliseconds.

parameters (NBV and mean global cortical thickness) between the groups ($p = 0.189$ and $p = 0.151$). Mean FA values extracted from the entire white matter after tissue segmentation were significantly reduced in patients compared to control subjects ($p = 0.01$). CSVD patients showed significantly impaired global cognitive performance and executive function as compared to control subjects ($p = 0.0001$ and $p = 0.002$). Table 1 summarizes the demographic baseline characteristics as well as results from structural imaging and cognitive assessment for both groups.

Global cortical DTI and qMRI parameters in patients and control subjects

Cortical diffusivity was significantly increased in patients compared to controls (MD: 1.0693 $10^{-3}mm^2s^{-1}$ ± 0.11214 $10^{-3}mm^2s^{-1}$ vs. 0.9921 $10^{-3}mm^2s^{-1}$ ± 0.07783 $10^{-3}mm^2s^{-1}$, $p = 0.015$; RD: 1.0552 $10^{-3}mm^2s^{-1}$ ± 0.10829 $10^{-3}mm^2s^{-1}$ vs. 0.9788 $10^{-3}mm^2s^{-1}$ ± 0.07388 $10^{-3}mm^2s^{-1}$, $p = 0.009$)

Furthermore, mean global cortical T_2 values showed a significant increase in CSVD patients as compared to control subjects (143.4 ms ± 25.90 ms vs. 131.6 ms ± 16.71 ms, $p = 0.034$). No significant differences were found for cortical FA (0.190 ± 0.0309 vs. 0.195 ± 0.0178, $p = 0.28$) as well as T_2* and $T_{2'}$ values (64.5 ms ± 11.10 ms vs. 59.9 ms ± 5.32 ms, $p = 0.137$; 169.8 ms ± 22.38 ms vs. 162.2 ms ± 22.17 ms, $p = 0.277$) between the groups.

Associations between cortical imaging parameters and the extent of white matter damage in CSVD patients

After controlling for age and sex by partial correlations, no significant associations with the mean Fazekas score were found for cortical MD and RD ($r = 0.225$, $p = 0.06$ and $p = 0.227$, $p = 0.059$),while cortical T_2 values correlated significantly with the mean Fazekas score ($r = 0.302$, $p = 0.025$) in the patient group. While cortical MD and RD values showed no significant correlations with the segmented WMH volume ($p = 0.293$ and $p = 0.282$), cortical T_2 values showed a significant positive signed correlation with the WMH volume ($r = 0.468$, $p = 0.002$, Fig. 3A). This correlation remained significant when cortical thickness was added as a nuisance variable ($r = 0.332$, $p = 0.037$). The averaged FA values obtained from the entire segmented WM (including the WMH) as a marker of axonal damage of the large WM fiber tracts were significantly

Table 1
Demographic baseline characteristics, results from structural imaging and cognitive assessment for patients and control subjects. Data are presented as mean ± SD unless indicated otherwise.

	CSVD patients (n = 33)	Control subjects (n = 16)	p-value
Age (years)	70.3 ± 10.55	70.6 ± 7.53	0.925
Female sex (%)	56.3	48.5	0.610
WMH volume, cm^3 (median) (IQR)	20.7 (26.5–16.7)	6.2 (8.9–3.9)	0.0001
Lacunes, n (median) (IQR)	1 (2–0)	0 (0–0)	0.0001
CMBs, n (median) (IQR)	0 (2–0)	0 (1–0)	0.006
NBV*	0.71 ± 0.030	0.72 ± 0.026	0.189
Global cortical thickness (mm)	2.41 ± 0.119	2.44 ± 0.087	0.151
Global white matter FA	0.38 ± 0.053	0.41 ± 0.042	0.01
Global cognitive composite (z-score)**	−0.69 ± 0.825	0.30 ± 0.552	0.0001
Executive function composite (z-score)**	−0.30 ± 0.864	0.55 ± 0.870	0.002

*: expressed as a fraction of the total incranial volume (TIV).
** averaged z-scores across the included subtests, which were adjusted for age, sex and years of education. WMH: white matter hyperintensities; IQR: interquartile range; CMB: cerebral microbleed; NBV: normalized brain volume; FA: fractional anisotropy.

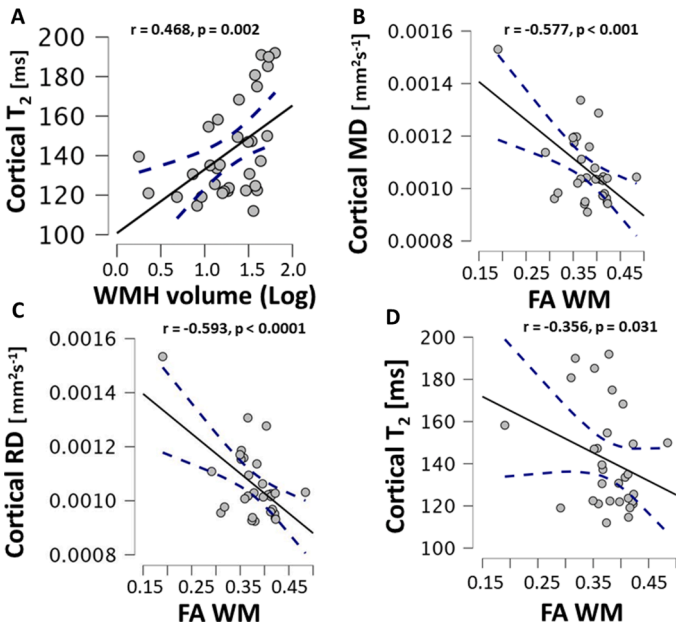

Fig. 3. Scatterplots illustrating the relationship of cortical imaging parameters and (micro-) structural WM damage. A: Association between cortical T_2 and WMH volume. B-D: Relationship of cortical diffusivity (B, C) and cortical T_2 values (D) with the averaged FA as a marker for axonal damage to WM fiber tracts. A line of best fit for the linear relationship between the two variables as well as the 95 % confidence interval are shown in each graph. MD: mean diffusivity; RD: radial diffusivity; mm: millimeters; s: seconds; ms: milliseconds. Correlation coefficients reflect partial correlations corrected for age and sex.

negatively correlated with both the averaged cortical diffusivity (MD: $r = -0.577$, $p = 0.001$; RD: $r = -0.593$, $p < 0.0001$) and the averaged cortical T_2 values ($r = -0.356$, $p = 0.031$) (Fig. 3B-D). All correlations were controlled for age and sex.

Associations of imaging parameters with cognitive performance and correlations between imaging parameters in CSVD patients

In order to investigate the potential relevance of cortical qMRI/DTI parameters and structural imaging parameters for the impaired cognitive performance detected in CSVD patients as compared to control subjects, we assessed the association of each cognitive composite score with the respective imaging parameters in the group of CSVD patients. Apart from the NBV, none of the investigated imaging parameters (including cortical thickness as well as global cortical diffusivity and global cortical T_2) showed a significant association with the cognitive composite scores. For the executive function composite score, there was a moderate significant positive correlation with the NBV ($r = 0.382$, $p = 0.025$), even after inclusion of the WMH volume as a nuisance variable ($r = 0.386$, $p = 0.026$). For the global cognitive composite score, a strongly significant positive correlation with the NBV was found ($r = 0.536$, $p = 0.002$), which remained significant when controlling for the WMH volume ($r = 0.533$, $p = 0.0025$). While no significant associations were found between cortical T_2 values and cortical MD and RD (trend to significance with $p = 0.077$ and $p = 0.067$, respectively), both T_2 and cortical diffusivity showed a significant negative correlation with cortical thickness ($p < 0.01$), which was also negatively correlated with the WMH volume ($r = -0.37$, $p < 0.05$). Neither cortical thickness nor the microstructural imaging parameters (including cortical diffusivity and T_2 as well as white matter FA) showed significant associations with the NBV. Detailed results for correlations, both between imaging parameters and between imaging parameters and cognitive measures are provided in Fig. 4.

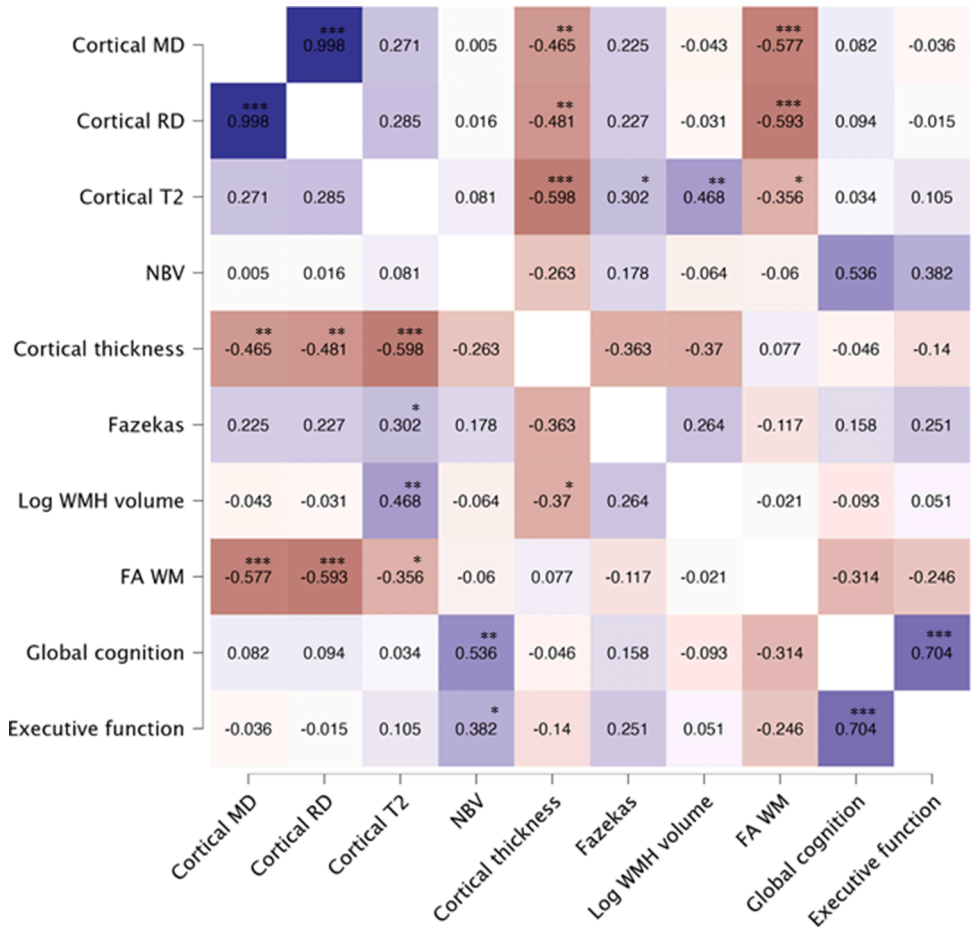

Fig. 4. Correlation matrix displaying correlation coefficients (partial r, corrected for age and sex) for associations between imaging parameters as well as between imaging parameters and cognition. Whereas neutral bright colours denote weak correlations, stronger shades of blue indicate positive correlations and stronger shades of red indicate negative correlations. Significant correlations are flagged with asterisks. *: $p < 0.05$; **:$p < 0.01$; ***: $p < 0.001$; MD: mean diffusivity; RD: radial diffusivity; NBV: normalized brain volume; WMH: white matter hyperintensity; FA: fractional anisotropy; WM; white matter.

Discussion

In this study, microstructural involvement of the cerebral cortex was investigated in CSVD patients without cerebral or cortical atrophy in comparison to a group of healthy control subjects, using cortical DTI and quantitative mapping of transverse relaxation times, along with a surface-based analysis approach. CSVD patients showed significantly impaired white matter microstructure (reduced FA) as a major determinant of cognitive function in CSVD [3] as well as significantly worse executive functioning and global cognitive performance without significant reductions in brain volume and global cortical thickness compared to healthy control subjects (Table 1). Among the investigated diffusion and qMRI parameters, cortical mean and radial diffusivity (MD and RD) as well as T_2 values showed significant differences, being increased in CSVD patients as compared to control subjects. In contrast, no significant differences regarding cortical FA as well as cortical T_2* and $T_{2'}$ values were found between the two groups.

Mean values of cortical DTI parameters as derived in our study are comparable to values reported in previous studies using DTI for the investigation of the cortical microstructure in patients with subcortical brain lesions [15,36,37]. In our CSVD patient cohort, cortical FA values were not significantly altered in patients compared to control subjects. However, since neuronal structures (e.g. cell bodies) in the cerebral cortex are largely isotropic, neuronal tissue loss would not necessarily be expected to cause to measurable alterations of cortical FA. For this reason, FA might be a less sensitive parameter for the detection of pathological alterations of the cortical microstructure. In contrast, we found increased cortical diffusivity in patients, indicating an alteration of the interaction between water molecules and microstructural boundaries in the cortical tissue of CSVD patients with a lower degree of hindrance of water diffusion [26-28,38]. Furthermore, cortical T_2 was significantly higher in CSVD patients than in controls. Quantitative T_2 mapping is sensitive to several distinct pathological alterations of the brain tissue microstructure, which include in particular demyelination, gliotic tissue conversion, and an increase of the tissue fluid content due to intra- and extracellular edema [17,18]. According to the pathological alterations of the cortical microstructure described both in experimental and MR imaging studies, one of the major causes potentially underlying increased cortical diffusivity and prolonged cortical T_2 in CSVD might be an elevated permeability or disruption of the blood-brain-barrier (BBB) [3,39-41] and the formation of myelin vacuoles with segmental edema [42]. A resulting enlargement of the extracellular space due to an interstitial edema yields both an increased cortical diffusivity and a prolonged cortical T_2 [17,18]. Widespread increases of the BBB permeability have been recently described within normal-appearing cortical tissue in patients with CSVD [41]. Furthermore, an impairment of the glymphatic clearance function leading to a failure of perivascular fluid transport and thus an increase of the interstitial fluid content is increasingly being proposed as a key mechanism in the CSVD pathophysiology [43,44]. Apart from a primary extracellular edema due to an impairment of the BBB or glymphatic dysfunction, the increase of cortical MD and RD as well as cortical T_2 values might be explained by a relative enlargement of the extracellular space because of neuronal atrophy or neuronal loss caused by microstructural damage and axonal

degeneration in major white matter fiber tracts. The degeneration of cortical tissue through microstructural "disconnection" of cortical neurons in the course of progressive white matter damage has been proposed as one of the pathophysiological key mechanisms by which CSVD affects the entire brain and causes cortical gray matter atrophy [6,12,45]. Both the extent of BBB impairment and cortical neuronal loss are commonly related to disease severity in terms of the overall lesion load [6,12,41,45]. Therefore, the significant group differences in cortical diffusivity and the positive association of cortical T_2 values with the WM lesion load (Fig. 3A) are compatible with the hypothesis of BBB leakage and neuronal loss as mechanisms driving increases of both cortical diffusivity and cortical T_2 values. Furthermore, the significant relationships of cortical diffusivity and cortical T_2 values with the global WM FA values (Fig. 3B-D) likewise support the hypothesis of axonal damage of the major WM fiber tracts with cortical microstructural neuronal loss through disconnection as an important mechanism, suggesting that microstructural cortical damage is closely related to an impaired WM integrity. Cortical thickness as a widely used parameter for cortical microstructural integrity is negatively associated with the WMH volume [11,12,35] (Fig. 4), but the relationship is strongly age-mediated [12-14,35]. In contrast, in this study the association of cortical T_2 values with the WMH volume remained significant after adjustment for age and sex (Fig. 3A), while the correlation of MD and RD values with the WMH was not statistically significant (Fig. 4). This finding might indicate that T_2 mapping reflects the actual CSVD-related microstructural tissue pathology more specifically and more independently of age than cortical thickness, and possibly also MD and RD, as suspected earlier [17]. Furthermore, since the association between cortical T_2 and WMH volume remained significant after controlling for cortical thickness, our results do not suggest that the correlation is only driven by cortical thinning and thus partial volume effects from the adjacent cerebrospinal fluid (CSF). In general, increases in cortical diffusivity and cortical T_2 most likely represent an earlier stage of cortical microstructural impairment, in contrast to cortical thinning which indicates tissue atrophy at a larger scale and thus a more advanced stage of cortical microstructural impairment. In general, this hypothesis would be supported by the significant correlations of cortical MD, RD and T_2 values with cortical thickness (Fig. 4), although it could only be confirmed in larger studies with a longitudinal design. The lack of significant associations between cortical diffusivity and T_2 and the differences between those imaging markers with regard to their association with microstructural WM damage and lesion load (Fig. 3, Fig. 4) may suggest different sensitivities to various aspects of cortical microstructural pathology, but this study was not powered to shed light on this question in a more detailed manner.

Quantitative T_2* is sensitive to the cortical myelin and iron content [46–49] and quantitative $T_{2'}$ is commonly considered a highly sensitive surrogate marker of tissue iron deposition due to the correction for inherent spin-spin effects in comparison to quantitative T_2* (with $1/T2' = 1/T2^* - 1/T2$) [48–51]. In addition, $T_{2'}$ can be used as a parameter of tissue oxygen metabolism since a local relative increase of deoxygenated haemoglobin leads to markedly reduced $T_{2'}$ values [18,52]. The lack of a significant difference of T_2* and $T_{2'}$ values between CSVD patients and control subjects suggests that changes in cortical myelination as well as in cortical iron deposition and cortical oxygenation do not play a relevant role in CSVD - at least in patients without significant cortical or whole-brain atrophy. However, especially T_2* and $T_{2'}$ are prone to artefacts induced by local field inhomogeneities complicating the investigation of the thin cortical layer. Therefore, the lack of a significant difference in cortical T_2* and $T_{2'}$ values between the groups should be interpreted with caution with respect to pathophysiological hypotheses.

Among the quantitative and structural imaging parameters investigated in this study, only the NBV was significantly associated with the executive functions and the global cognitive performance in CSVD. In line with the results of previous studies, our results suggest that brain atrophy determines cognitive impairment in elderly subjects with CSVD [7,53]. The relationship between brain atrophy and cognitive impairment is complex and is mediated by several factors including age, WMH load, (strategic) lacunes, CMBs, vascular risk factors and β−Amyloid deposition due to concomitant Alzheimer's pathology [54,55]. A longitudinal imaging study on CSVD patients investigating changes in diffusion and structural imaging described short-term changes in DTI parameters preceding (further) whole-brain atrophy and (progressive) cognitive deterioration [10]. Those findings suggest a sequence of CSVD-related pathological alterations of the tissue microstructure followed by tissue volume reduction and finally its clinical manifestations as cognitive impairment in multiple cognitive domains. In view of this well-documented pathophysiological course, the lack of a significant association of cortical diffusivity and cortical T_2 values with the cognitive performance is not entirely unexpected. Furthermore, of note, there was no significant difference in cortical thickness between CSVD patients and control subjects, despite marked differences in cognitive performance (Table 1). Changes of cortical thickness in CSVD, also with respect to their association with WMH volume and localization and their impact on cognitive status, seem to be heterogeneous and complex [9,11,12] and the role of cortical thinning for cognitive impairment and deterioration in CSVD is currently not entirely clear. In line with these observations, no significant association was found between cortical thickness and cognitive performance in our study, which generally questions the relevance of cortical microstructural for cognitive impairment in CSVD (at least at earlier stages) and makes the lack of a significant relationship of cortical diffusivity and cortical T_2 less surprising. In accordance with previous research, our results suggest that cognitive impairment in CSVD is mainly driven by subcortical WM pathology leading to an overall reduction of brain volume [3,7,8,10,53]. The increase of cortical diffusivity and the prolongation of cortical T_2 most likely represent an early impairment of the cortical microstructure related to progressive ischemic damage to the cerebral WM (Fig. 3). The additional impact of such alterations of the cortical microstructure in CSVD needs to be elucidated in future studies.

Limitations

The major limitation of this study is the rather small sample size. Furthermore, since this a cross-sectional study, we are not able to comment on the temporal dynamics of changes in cortical diffusivity and cortical T_2 values, their magnitude and how they relate to cerebral structural changes and clinical features of CSVD. With regard to the actual microstructural processes involved in cortical remodelling in CSVD, only pathophysiological assumptions can be made based on the changes observed in the employed DTI and qMRI parameters. Disentangling the contributions of BBB leakage and impaired glymphatic clearance function leading to primary increase of extracellular fluid content through interstitial edema and microstructural atrophy leading to a secondary increase of the tissue water fraction would require adding imaging modalities which allow for assessing the functionality of the BBB and the glymphatic system [41,44]. Moreover, despite the optimized coregistration and analysis method for the avoidance of partial volume effects, also in the light of the significant negative associations of cortical diffusivity and cortical T_2 with cortical thickness, we cannot fully exclude an influence of such on our results. Finally, the prevalence of typical CSVD-related imaging findings beyond WMH, such as lacunes and CMBs, was low in our cohort (Table 1). As the individual load of lacunar lesions is known to have a substantial impact on the cortical structure [56,57], the microstructural involvement might vary according to the CSVD phenotype and the predominant subcortical manifestation. This would be an intriguing question to investigate in future studies.

Conclusions

Cortical diffusivity and quantitative T_2 mapping are suitable to

detect microstructural involvement of the cortical grey matter in CSVD, even when no relevant cortical or whole-brain atrophy is present. Global cortical MD, RD and T_2 values are significantly associated with the WM lesion load and microstructural damage of WM tracts, which would be in line with progressive BBB leakage related to the overall disease severity and with the concept of cortical tissue damage because of disconnection through progressive disruption of fiber tracts in CSVD. Especially quantitative T_2 might be a promising imaging biomarker, which specifically reflects CSVD-related alterations of cortical microstructure and therefore could be used for monitoring disease progression or evaluating the effects of therapeutic interventions in clinical studies. Future longitudinal studies and larger sample sizes are warranted and required in order to assess the utility of quantitative T_2 as a predictor of (further) cognitive decline and cortical atrophy in CSVD.

CRediT authorship contribution statement

Annemarie Reiländer: Conceptualization, Data curation, Methodology, Project administration, Resources, Software, Visualization, Writing – review & editing. **Marlene Engel:** Data curation, Investigation, Methodology, Project administration, Software, Visualization, Writing – original draft, Writing – review & editing. **Ulrike Nöth:** Methodology, Project administration, Resources, Software, Supervision, Validation, Writing – review & editing. **Ralf Deichmann:** Methodology, Project administration, Resources, Software, Supervision, Validation, Writing – review & editing. **Manoj Shrestha:** Methodology, Resources, Software, Supervision, Writing – review & editing. **Marlies Wagner:** Conceptualization, Investigation, Methodology, Resources, Software, Supervision, Validation, Writing – original draft, Writing – review & editing. **René-Maxime Gracien:** Conceptualization, Data curation, Formal analysis, Investigation, Methodology, Supervision, Validation, Writing – original draft, Writing – review & editing. **Alexander Seiler:** Conceptualization, Data curation, Formal analysis, Funding acquisition, Methodology, Project administration, Supervision, Validation, Visualization, Writing – original draft, Writing – review & editing.

Declaration of competing interest

The authors declare that they have no known competing financial interests or personal relationships that could have appeared to influence the work reported in this paper.

Funding

This work was supported by the Else-Kröner-Fresenius-Stiftung (research grant to RMG and AS) and by the Clinician Scientist program of the Goethe University Frankfurt/Faculty of Medicine (research grant to AS).

Acknowledgements

None.

References

[1] L. Pantoni, Cerebral small vessel disease: from pathogenesis and clinical characteristics to therapeutic challenges, Lancet Neurol. 9 (2010) 689–701, https://doi.org/10.1016/S1474-4422(10)70104-6.
[2] M. Dichgans, D. Leys, Vascular Cognitive Impairment, Circ. Res. 120 (2017) 573–591, https://doi.org/10.1161/CIRCRESAHA.116.308426.
[3] M. Duering, S. Finsterwalder, E. Baykara, et al., Free water determines diffusion alterations and clinical status in cerebral small vessel disease, Alzheimers. Dement. 14 (2018) 764–774, https://doi.org/10.1016/j.jalz.2017.12.007.
[4] M. Pasi, C. Cordonnier, Clinical relevance of cerebral small vessel diseases, Stroke 51 (2020) 47–53, https://doi.org/10.1161/STROKEAHA.119.024148.
[5] J.M. Wardlaw, E.E. Smith, G.J. Biessels, et al., Neuroimaging standards for research into small vessel disease and its contribution to ageing and neurodegeneration, Lancet Neurol. 12 (2013) 822–838, https://doi.org/10.1016/S1474-4422(13)70124-8.
[6] C. Lambert, P. Benjamin, E. Zeestraten, et al., Longitudinal patterns of leukoaraiosis and brain atrophy in symptomatic small vessel disease, Brain 139 (2016) 1136–1151, https://doi.org/10.1093/brain/aww009.
[7] A. Nitkunan, S. Lanfranconi, R.A. Charlton, et al., Brain atrophy and cerebral small vessel disease: a prospective follow-up study, Stroke 42 (2011) 133–138, https://doi.org/10.1161/STROKEAHA.110.594267.
[8] R.P. Kloppenborg, P.J. Nederkoorn, A.M. Grool, et al., Cerebral small-vessel disease and progression of brain atrophy: the SMART-MR study, Neurology. 79 (2012) 2029–2036, https://doi.org/10.1212/WNL.0b013e3182749f02.
[9] R. Peres, F. De Guio, H. Chabriat, et al., Alterations of the cerebral cortex in sporadic small vessel disease: a systematic review of in vivo MRI data, J. Cereb. Blood Flow Metab. 36 (2016) 681–695, https://doi.org/10.1177/0271678X15625352.
[10] P. Benjamin, E. Zeestraten, C. Lambert, et al., Progression of MRI markers in cerebral small vessel disease: sample size considerations for clinical trials, J. Cereb. Blood Flow Metab. 36 (2016) 228–240, https://doi.org/10.1038/jcbfm.2015.113.
[11] C. Lambert, J. Sam Narean, P. Benjamin, et al., Characterising the grey matter correlates of leukoaraiosis in cerebral small vessel disease, Neuroimage Clin. 9 (2015) 194–205, https://doi.org/10.1016/j.nicl.2015.07.002.
[12] A.M. Tuladhar, A.T. Reid, E. Shumskaya, et al., Relationship between white matter hyperintensities, cortical thickness, and cognition, Stroke 46 (2015) 425–432, https://doi.org/10.1161/STROKEAHA.114.007146.
[13] T. Liu, P.S. Sachdev, D.M. Lipnicki, et al., Limited relationships between two-year changes in sulcal morphology and other common neuroimaging indices in the elderly, Neuroimage 83 (2013) 12–17, https://doi.org/10.1016/j.neuroimage.2013.06.058.
[14] P. Kochunov, P.M. Thompson, T.R. Coyle, et al., Relationship among neuroimaging indices of cerebral health during normal aging, Hum. Brain Mapp. 29 (2008) 36–45, https://doi.org/10.1002/hbm.20369.
[15] B. Stock, M. Shrestha, A. Seiler, et al., Distribution of Cortical Diffusion Tensor Imaging Changes in Multiple Sclerosis, Front. Physiol. 11 (2020) 116, https://doi.org/10.3389/fphys.2020.00116.
[16] L.J. Edwards, E. Kirilina, S. Mohammadi, et al., Microstructural imaging of human neocortex in vivo, Neuroimage 182 (2018) 184–206, https://doi.org/10.1016/j.neuroimage.2018.02.055.
[17] A. Brandhofe, C. Stratmann, J.R. Schure, et al., T2 relaxation time of the normal-appearing white matter is related to the cognitive status in cerebral small vessel disease, J. Cereb. Blood Flow Metab. 41 (2021) 1767–1777, https://doi.org/10.1177/0271678X20972511.
[18] M. Wagner, M. Helfrich, S. Volz, et al., Quantitative T2, T2*, and T2′ MR imaging in patients with ischemic leukoaraiosis might detect microstructural changes and cortical hypoxia, Neuroradiology. 57 (2015) 1023–1030, https://doi.org/10.1007/s00234-015-1565-x.
[19] S.M. Smith, M. Jenkinson, M.W. Woolrich, et al., Advances in functional and structural MR image analysis and implementation as FSL, Neuroimage 23 (Suppl 1) (2004) S208–S219, https://doi.org/10.1016/j.neuroimage.2004.07.051.
[20] B. Fischl, D.H. Salat, A.J. van der Kouwe, et al., Sequence-independent segmentation of magnetic resonance images, Neuroimage 23 (Suppl 1) (2004) S69–S84, https://doi.org/10.1016/j.neuroimage.2004.07.016.
[21] J.L. Andersson, S. Skare, J. Ashburner, How to correct susceptibility distortions in spin-echo echo-planar images: application to diffusion tensor imaging, Neuroimage 20 (2003) 870–888, https://doi.org/10.1016/S1053-8119(03)00336-7.
[22] S.M Smith, Fast robust automated brain extraction, Hum Brain Mapp. 17 (2002) 143–155, https://doi.org/10.1002/hbm.10062.
[23] J.L.R. Andersson, S.N. Sotiropoulos, An integrated approach to correction for off-resonance effects and subject movement in diffusion MR imaging, Neuroimage 125 (2016) 1063–1078, https://doi.org/10.1016/j.neuroimage.2015.10.019.
[24] T.E. Behrens, M.W. Woolrich, M. Jenkinson, et al., Characterization and propagation of uncertainty in diffusion-weighted MR imaging, Magn. Reson. Med. 50 (2003) 1077–1088, https://doi.org/10.1002/mrm.10609.
[25] T.E. Behrens, H.J. Berg, S. Jbabdi, et al., Probabilistic diffusion tractography with multiple fibre orientations: what can we gain? Neuroimage 34 (2007) 144–155, https://doi.org/10.1016/j.neuroimage.2006.09.018.
[26] E.A. Zeestraten, P. Benjamin, C. Lambert, et al., Application of diffusion tensor imaging parameters to detect change in longitudinal studies in cerebral small vessel disease, PLoS. One 11 (2016) e0147836, https://doi.org/10.1371/journal.pone.0147836.
[27] S.K. Song, S.W. Sun, W.K. Ju, et al., Diffusion tensor imaging detects and differentiates axon and myelin degeneration in mouse optic nerve after retinal ischemia, Neuroimage 20 (2003) 1714–1722, https://doi.org/10.1016/j.neuroimage.2003.07.005.
[28] S.K. Song, S.W. Sun, M.J. Ramsbottom, et al., Dysmyelination revealed through MRI as increased radial (but unchanged axial) diffusion of water, Neuroimage 17 (2002) 1429–1436, https://doi.org/10.1006/nimg.2002.1267.
[29] U. Noth, S. Volz, E. Hattingen, et al., An improved method for retrospective motion correction in quantitative T2* mapping, Neuroimage 92 (2014) 106–119, https://doi.org/10.1016/j.neuroimage.2014.01.050.
[30] Fischl B. FreeSurfer. neuroimage 2012; 62: 774–781. Historical Article Research Support, N.I.H., Extramural, Research Support, Non-U.S. Gov't, Review 2012/01/18. 10.1016/j.neuroimage.2012.01.021.
[31] Greve D.N. and Fischl B. Accurate and robust brain image alignment using boundary-based registration. Neuroimage 2009; 48: 63–72. Evaluation Study Research Support, N.I.H., Extramural Research Support, Non-U.S. Gov't. DOI: 10.1016/j.neuroimage.2009.06.060.

[32] J.C. Morris, R.C. Mohs, H. Rogers, et al., Consortium to establish a registry for Alzheimer's disease (CERAD) clinical and neuropsychological assessment of Alzheimer's disease, Psychopharmacol. Bull. 24 (1988) 641–652.
[33] M.M. Ehrensperger, M. Berres, K.I. Taylor, et al., Early detection of Alzheimer's disease with a total score of the German CERAD, J. Int. Neuropsychol. Soc. 16 (2010) 910–920, https://doi.org/10.1017/S1355617710000822.
[34] M.J. Chandler, L.H. Lacritz, L.S. Hynan, et al., A total score for the CERAD neuropsychological battery, Neurology. 65 (2005) 102–106, https://doi.org/10.1212/01.wnl.0000167607.63000.38.
[35] A.T. Reid, A.G. van Norden, K.F. de Laat, et al., Patterns of cortical degeneration in an elderly cohort with cerebral small vessel disease, Hum. Brain Mapp. 31 (2010) 1983–1992, https://doi.org/10.1002/hbm.20994.
[36] K.M. Hasan, I.S. Walimuni, H. Abid, et al., Multi-modal quantitative MRI investigation of brain tissue neurodegeneration in multiple sclerosis, J. Magn. Reson. Imaging 35 (2012) 1300–1311, https://doi.org/10.1002/jmri.23539.
[37] P. Tortorella, M.A. Rocca, D.M. Mezzapesa, et al., MRI quantification of gray and white matter damage in patients with early-onset multiple sclerosis, J. Neurol. 253 (2006) 903–907, https://doi.org/10.1007/s00415-006-0129-8.
[38] M. Filippi, G. Iannucci, M. Cercignani, et al., A quantitative study of water diffusion in multiple sclerosis lesions and normal-appearing white matter using echo-planar imaging, Arch. Neurol. 57 (2000) 1017–1021, https://doi.org/10.1001/archneur.57.7.1017.
[39] S. Munoz Maniega, F.M. Chappell, M.C. Valdes Hernandez, et al., Integrity of normal-appearing white matter: influence of age, visible lesion burden and hypertension in patients with small-vessel disease, J. Cereb. Blood Flow Metab. 37 (2017) 644–656, https://doi.org/10.1177/0271678X16635657.
[40] M. Ghosh, M. Balbi, F. Hellal, et al., Pericytes are involved in the pathogenesis of cerebral autosomal dominant arteriopathy with subcortical infarcts and leukoencephalopathy, Ann. Neurol. 78 (2015) 887–900, https://doi.org/10.1002/ana.24512.
[41] C.E. Zhang, S.M. Wong, H.J. van de Haar, et al., Blood-brain barrier leakage is more widespread in patients with cerebral small vessel disease, Neurology. 88 (2017) 426–432, https://doi.org/10.1212/WNL.0000000000003556.
[42] E. Cognat, S. Cleophax, V. Domenga-Denier, et al., Early white matter changes in CADASIL: evidence of segmental intramyelinic oedema in a pre-clinical mouse model, Acta Neuropathol. Commun. 2 (2014) 49, https://doi.org/10.1186/2051-5960-2-49.
[43] H. Mestre, S. Kostrikov, R.I. Mehta, et al., Perivascular spaces, glymphatic dysfunction, and small vessel disease, Clin. Sci. (Lond.) 131 (2017) 2257–2274, https://doi.org/10.1042/CS20160381.
[44] W. Zhang, Y. Zhou, J. Wang, et al., Glymphatic clearance function in patients with cerebral small vessel disease, Neuroimage 238 (2021) 118257, https://doi.org/10.1016/j.neuroimage.2021.118257.
[45] M. Pasi, I.W. van Uden, A.M. Tuladhar, et al., White Matter microstructural damage on diffusion tensor imaging in cerebral small vessel disease: clinical consequences, Stroke 47 (2016) 1679–1684, https://doi.org/10.1161/STROKEAHA.115.012065.
[46] M. Fukunaga, T.Q. Li, P. van Gelderen, et al., Layer-specific variation of iron content in cerebral cortex as a source of MRI contrast, Proc. Natl. Acad. Sci. U.S.A 107 (2010) 3834–3839, https://doi.org/10.1073/pnas.0911177107.
[47] D. Carey, F. Caprini, M. Allen, et al., Quantitative MRI provides markers of intra-, inter-regional, and age-related differences in young adult cortical microstructure, Neuroimage 182 (2018) 429–440, https://doi.org/10.1016/j.neuroimage.2017.11.066.
[48] A.M. Daugherty, N. Raz, Appraising the Role of Iron in Brain Aging and Cognition: promises and Limitations of MRI Methods, Neuropsychol. Rev. 25 (2015) 272–287, https://doi.org/10.1007/s11065-015-9292-y.
[49] G.A. Lodygensky, J.P. Marques, R. Maddage, et al., In vivo assessment of myelination by phase imaging at high magnetic field, Neuroimage 59 (2012) 1979–1987, https://doi.org/10.1016/j.neuroimage.2011.09.057.
[50] E.M. Haacke, N.Y. Cheng, M.J. House, et al., Imaging iron stores in the brain using magnetic resonance imaging, Magn. Reson. Imaging 23 (2005) 1–25, https://doi.org/10.1016/j.mri.2004.10.001.
[51] A. Seiler, S. Schongrundner, B. Stock, et al., Cortical aging - new insights with multiparametric quantitative MRI, Aging (Albany. NY) 12 (2020) 16195–16210, https://doi.org/10.18632/aging.103629.
[52] A. Seiler, N.P. Blockley, R. Deichmann, et al., The relationship between blood flow impairment and oxygen depletion in acute ischemic stroke imaged with magnetic resonance imaging, J. Cereb. Blood Flow Metab. 39 (2019) 454–465, https://doi.org/10.1177/0271678X17732448.
[53] H. Jokinen, J. Lipsanen, R. Schmidt, et al., Brain atrophy accelerates cognitive decline in cerebral small vessel disease: the LADIS study, Neurology. 78 (2012) 1785–1792, https://doi.org/10.1212/WNL.0b013e3182583070.
[54] R. Heinen, O.N. Groeneveld, F. Barkhof, et al., Small vessel disease lesion type and brain atrophy: the role of co-occurring amyloid, Alzheimers. Dement. (Amst) 12 (2020) e12060, https://doi.org/10.1002/dad2.12060.
[55] F. De Guio, M. Duering, F. Fazekas, et al., Brain atrophy in cerebral small vessel diseases: extent, consequences, technical limitations and perspectives: the HARNESS initiative, J. Cereb. Blood Flow Metab. 40 (2020) 231–245, https://doi.org/10.1177/0271678X19888967.
[56] M. Duering, R. Righart, E. Csanadi, et al., Incident subcortical infarcts induce focal thinning in connected cortical regions, Neurology. 79 (2012) 2025–2028, https://doi.org/10.1212/WNL.0b013e3182749f39.
[57] B. Cheng, R. Schulz, M. Bonstrup, et al., Structural plasticity of remote cortical brain regions is determined by connectivity to the primary lesion in subcortical stroke, J. Cereb. Blood Flow Metab. 35 (2015) 1507–1514, https://doi.org/10.1038/jcbfm.2015.74.